Volume 215 • Number 8 • April 25, 2014

www.mcp-journal.de

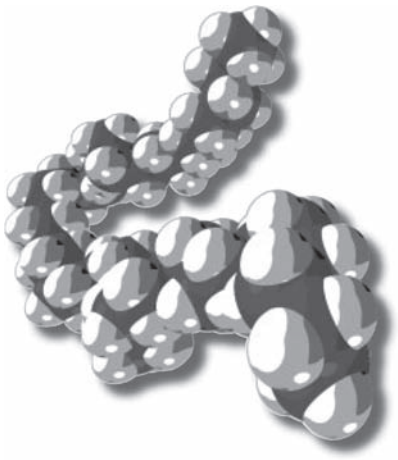

Macromolecular Chemistry and Physics

Founded by Hermann Staudinger

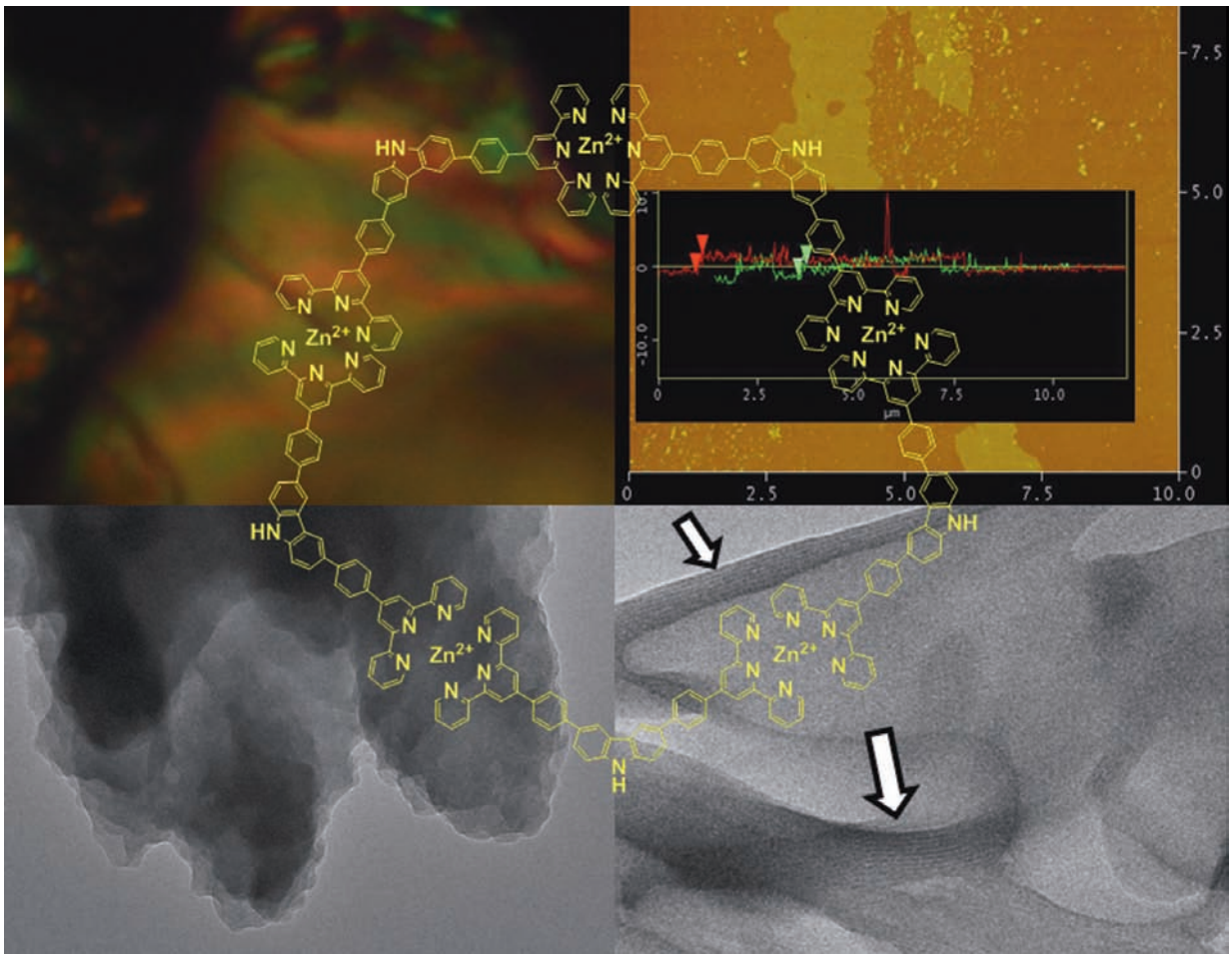

8/2014

WILEY-VCH

Influence of H-Bonding on Self-Assembly and Tunable Dual-Emission of Carbazole-Based Zn(II)-Terpyridine Metallocycles

Yang Gao, Tingchao He, Peng Hu, Teck Ming Koh, Handong Sun, Andrew C. Grimsdale*

Two carbazole derivatives with terpyridine units attached to the 3,6-positions are synthesized, **1** with a hydrogen at the 9-position and **2** bearing a dodecyl chain there, to evaluate the influence of H-bonds on their self-assembly behavior with metal ions. The unalkylated derivative **1** assembles with zinc ions to form a single product identified by NMR, electrospray ionisation mass spectrometry (ESI-MS), and X-ray photoelectron spectroscopy (XPS) as a pentametric metallocycle (**Zn-1**), whereas **2** forms a mixture of two assemblies (**Zn-2**). The pentamer **Zn-1** shows tunable dual emission in the blue and green regions by varying the solvent and excitation wavelength, and molecular packing studies by powder X-ray diffractometry (XRD), transmission electron microscopy (TEM), polarising optical microscopy (POM), and atomic force microscopy (AFM) reveals a high propensity to form ordered layers. A fluorescence quenching experiment of electron-rich **Zn-1** with C_{60} shows a high association constant of $K_{sv} = 3.2 \times 10^5$ M^{-1}, suggesting effective charge transfer between **Zn-1** and C_{60} molecules.

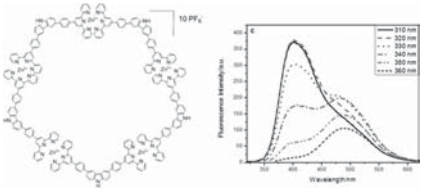

1. Introduction

Metallosupramolecular structures[1] have been a subject of intense research interest due to their fascinating physical and chemical properties. Coordination-driven assembly of terpyridine-based ligands[2] with metal ions has proved to be a versatile method, which has, for example, been used to form various aesthetically pleasant well-defined structures by Newkome et al., variously using two components[3,4] or multiple components,[5] in 2D[6] or 3D[7] layouts, and through one-pot[4] or stepwise[8–10] synthesis. Incorporation of organic chromophores into such defined assemblies to form organic–inorganic hybrid materials is of great interest due to their properties as the combination of the defined structures and the metal–ligand interactions produces novel optical and electronic properties, with potential applications in dye-sensitized solar cells (DSSC),[11] nonlinear optical limiting,[12] light-harvesting prototypes,[13,14] and so on. One type of material that could be exploited is supramolecular macrocycles based upon carbazole. Carbazole-based materials, due to their strong blue fluorescence and highly efficient hole transport properties, have been widely used in optoelectronic devices such as organic light-emitting diodes (OLED),[15] organic field electronic transistors (OFET),[16,17] and photovoltaic

Y. Gao, P. Hu, T. M. Koh, Prof. A. C. Grimsdale
School of Materials Science and Engineering, Nanyang Technological University, 50 Nanyang Avenue
Singapore 639798, Singapore
E-mail: acgrimsdale@ntu.edu.sg
Dr. T. He, Prof. H. Sun
Division of Physics and Applied Physics, School of Physical and Mathematical Sciences, Nanyang Technological University, Nanyang Link 21
Singapore 637371, Singapore

DOI: 10.1002/macp.201300737

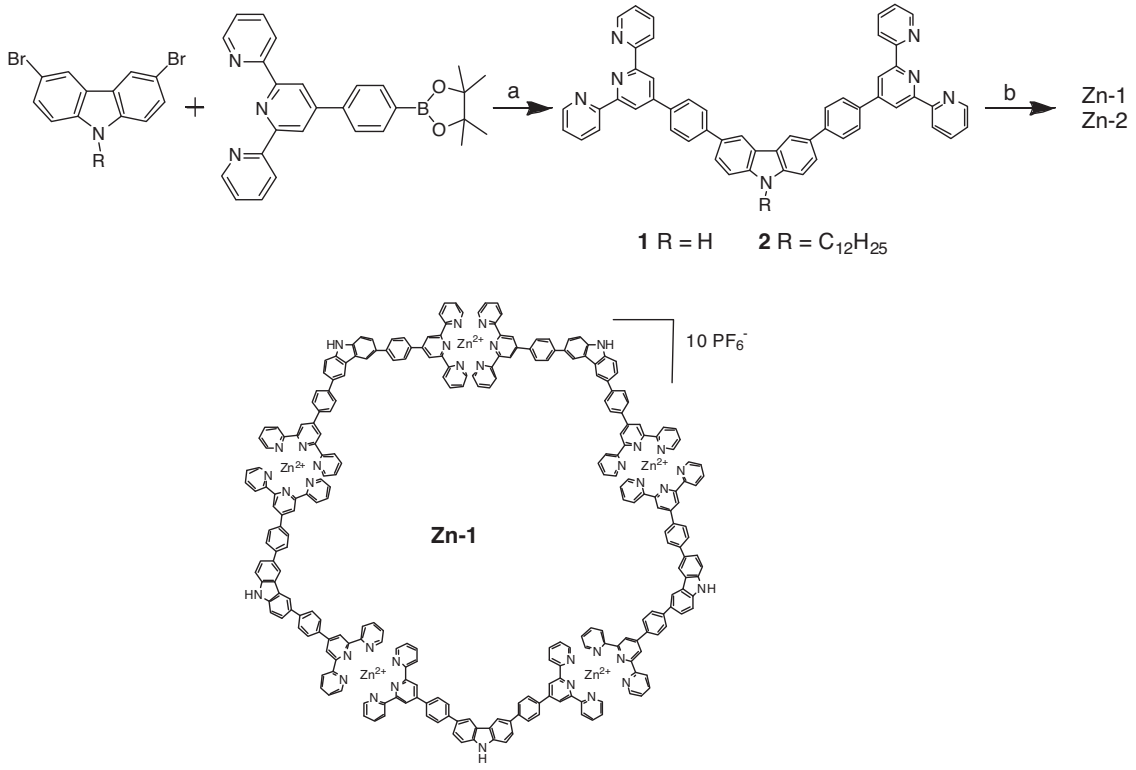

Figure 1. Synthetic schemes for ligands and metallocycles with Zn(II) ions, a: $Pd(PPh_3)_4$, K_2CO_3 (2 M), toluene for **1**, THF for **2**, reflux, 3–5 d; b: NMP, 100 °C, 48 h.

devices.[18–20] The device performance depends heavily on the morphology of active layers, which can be tuned by molecular design and intermolecular interactions with self-assembly methodology often applied to afford ordered structures. An exquisite example was the columnar assembly[21] of conjugated polycarbazole with good theoretical hole transport property.[22] The pentameric assembly of bisterpyridine ligands incorporating a carbazole chromophore (3,6-di([2,2′:6′,2″-terpyridin]-4′-yl)-9-hexyl-9H-carbazole) with a range of metal ions [Ru(II), Fe(II), Zn(II)] has been reported in 2005,[11] but to the best of our knowledge, the intermolecular interactions between such terpyridine-based metallo-structures and their assembly in concentrated states has yet not been reported. Thus, bottom-up assembly of such blocks to ordered structures in higher dimensions aroused our interest (taking stepwise formation of MOF as an example,[23] especially when chromophores or charge transport units could be incorporated to investigate the energy or charge transfer. H-bond facilitated self-assembly appears commonly in nature and in artificially designed systems, so we designed two carbazole derivatives [**1**, 3,6-bis(4-([2,2′:6′,2″-terpyridin]-4′-yl) phenyl)-9H-carbazole; **2**, 3,6-bis(4-([2,2′:6′,2″-terpyridin]-4′-yl)phenyl)-9-dodecyl-9H-carbazole]. The introduction of a dodecyl chain at N-position in **2** results in the disappearance of H-bond interaction, which exists in the ligand **1** with secondary amine (NH) functional group, enabling us to evaluate the influence of H-bonding upon their assembly with Zn(II) ions, and to study the photophysical, electrochemical, and molecular packing features of their assemblies.

2. Results and Discussion

2.1. Synthesis and Structure Characterization

The two ditopic terpyridine ligands were synthesized through Suzuki coupling in refluxing toluene or tetrahydrofuran (THF) of 4′-(4-(4,4,5,5-tetramethyl-1,3,2-dioxaborolan-2-yl)phenyl)-2,2′:6′,2″-terpyridine with 3,6-dibromo-9H-carbazole and 3,6-dibromo-9-dodecyl-9H-carbazole (Figure 1), respectively, and purified by alumina chromatography to afford off-white powders in moderate yield (**1**, 45%; **2**, 28%). The chemical structures were confirmed by ^1H NMR ($CDCl_3$) and MALDI-TOF-MS. Characteristic singlet 3′,5′-tpyH signals (**1,** 8.76 ppm; **2**, 8.85 ppm) of terpyridine and 4Ar–H in carbazole (**1**, 7.42 ppm (d); **2**, 8.49 ppm (s)) in 2:1 ratio, and 4.39 ppm (t) for NCH_2 in **2** (half amount of the terpyridine H-atoms) were in accordance with the supposed chemical composition (Figure 2). Moreover, the carbazole signals in **1** appeared at lower ppm than that of **2,** due to the stronger shielding effect of lone pair electrons of unsubstituted N

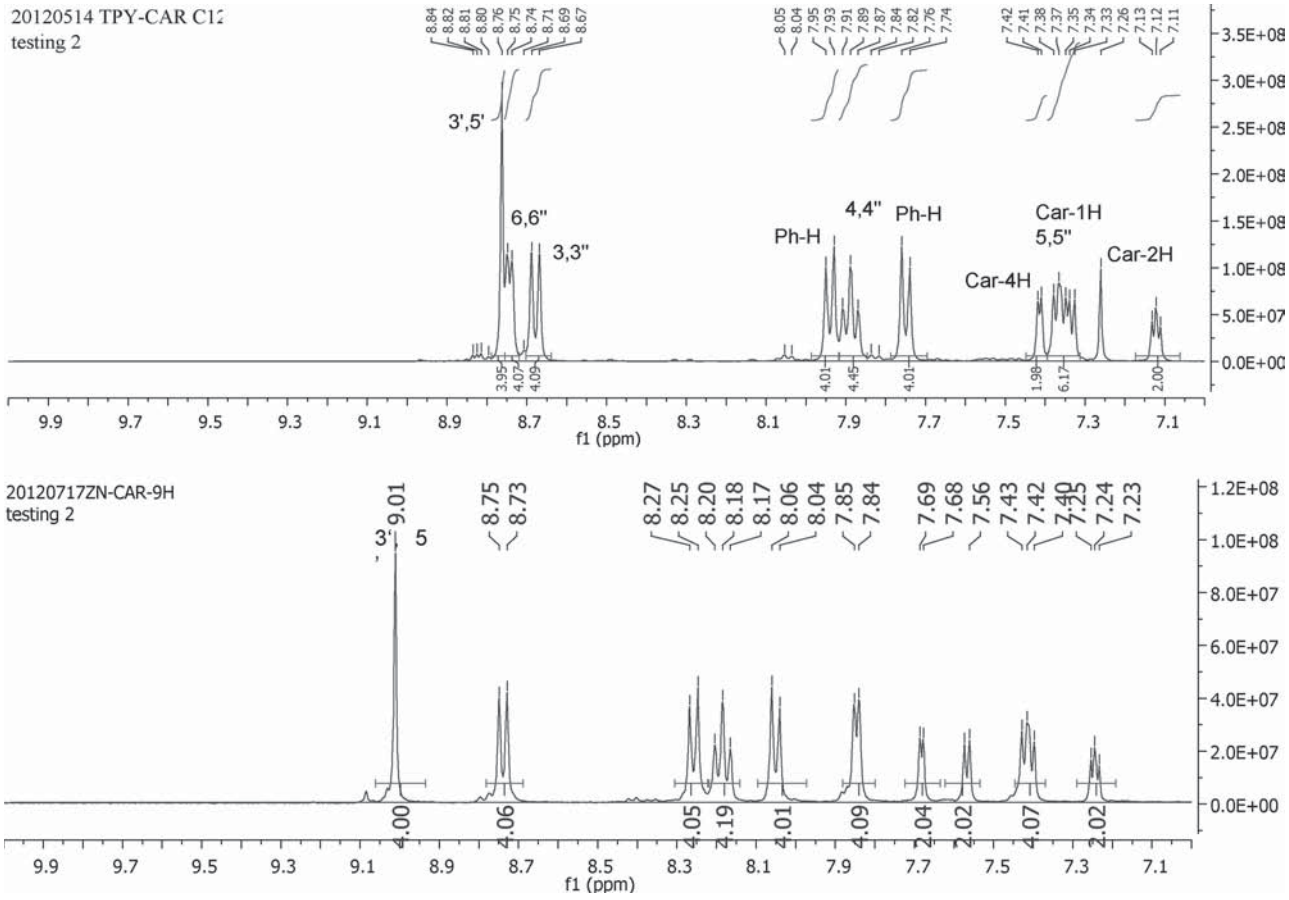

Figure 2. ^{1}H NMR spectra of metal-free ligand **1** ($CDCl_3$) and **Zn-1** (d_3-ACN).

atom in the former. In mass spectra, a negative-charged entity at *m/z* 780.40 $[M–H]^-$ was observed for **1**, and a positively charged entity at 951.16 $[M+H]^+$ for **2**.

The complexation was carried out by reaction of one equiv. of Zn(II) ions with the ditopic ligands in hot *N*-methyl-2-pyrrolidone (NMP) for 48 h, followed by counterion exchange with an excess amount of ammonium hexafluorophosphate. And the selection of NMP as solvent was due to the good dissolving ability for both the ligands and the metal ion precursor zinc acetate dihydrate ($Zn(OAc)_2{\cdot}2H_2O$), compared with limited solubility of **1** in other commonly used solvent such as acetonitrile (ACN), acetone, or dichloromethane/methanol (DCM/MeOH) mixture. The crude products were facilely collected by precipitating the reaction mixture from MeOH, purified by thorough washing of the precipitate with hot DCM and then MeOH, to give the complexes in moderate yield (**Zn-1**, 29%; **Zn-2**, 23%), in contrast to literature-reported column purification for similar structures. The structures were confirmed by ^{1}H NMR, electrospray ionisation mass spectrometry (ESI-MS), and X-ray photoelectron spectroscopy (XPS). The ^{1}H NMR (d3-ACN) signals of both **Zn-1** and **Zn-2** showed well-defined splitting patterns, which implied the existence of symmetric metallocyclic structures rather than linear oligomers, which would show broad structureless signals. Compared with the uncomplexed ligands, the upfield shift of doublet at 7.85 ppm for 6′,6″-tpyH ($\Delta\delta$ = –0.90 ppm) and downfield shift for the singlet at 9.00 ppm for 3′,5′-tpyH ($\Delta\delta$ = 0.25 ppm) in **Zn-1** (Figure 2) proved the occurrence of complexation and the appearance of one symmetrical metallocycle; while in **Zn-2** (Figure 3), two pairs of signals at 7.93 ppm ($\Delta\delta$ = –0.85 ppm) and 7.87 ppm ($\Delta\delta$ = –0.91 ppm) doublet for 6′,6″-tpyH, and 9.11 ppm ($\Delta\delta$ = 0.25 ppm) and 9.09 ppm ($\Delta\delta$ = 0.23 ppm) singlet for 3′,5′-tpyH appeared in a 3:1 ratio, indicating the coexistence of two metallocycles, which we were unable to separate. In ESI-MS for **Zn-1** (Figure S1, Supporting Information), multiply charged species appeared with charges ranging from +3 to +10, formed probably by combinational loss of H^+, PF_6^-, F^-, and PF_5,[24] which were consistent with a pentagonal assembly. The weak mass signals for **Zn-2** were not identifiable, but the aromatic NMR signals of the major component match those of **Zn-1** in chemical shifts suggesting it is also a pentamer. The minor component has slightly shielded signals for the 3′ and 5′ protons and we suggest this is consistent

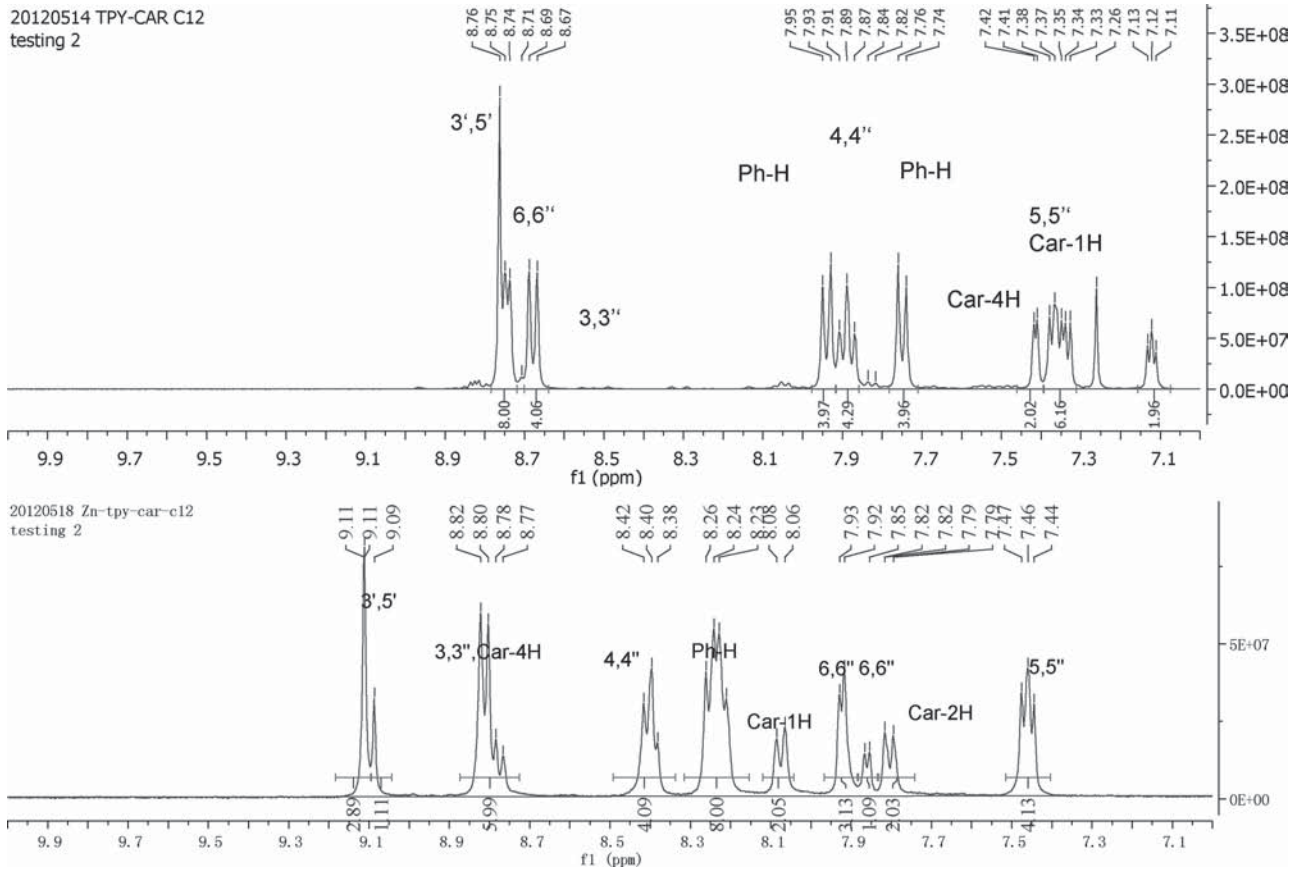

Figure 3. ^{1}H NMR spectra of metal-free ligand **2** ($CDCl_3$) and **Zn-2** (d_3-ACN).

with its possessing a less planar conformation bringing these protons into the shielding cone of a nearby aromatic ring. As a tetramer would be less planar than a hexamer, we tentatively suggest the minor component is a tetramer. Further studies are underway to attempt to elucidate the structure of this minor component of **Zn-2**. The complexation and single metallocycle structure of **Zn-1** was further confirmed by XPS, which showed signals at 1023.2 and 1046.0 eV for Zn $2p^{2/3}$ and $2p^{1/2}$ electrons, and a corresponding N 1s peak at 401.40 eV[9] (Figure S2, Supporting Information). The different assembly behaviors can be explained by the different solubility of the ligands and their complexes, as complexes of **2** should be more soluble than those of **1** due to the dodecyl chains and inability to form H-bond via the NH groups. As a result, complexes of **2** with Zn(II) may be more labile as they dissolve more readily and so can equilibrate in solution unlike a kinetically formed pentamer **Zn-1**, which is less soluble due in part to intermolecular H-bonding.

2.2. Photophysical Properties

The photophysical properties were evaluated by UV–vis absorption and fluorescence. **1** and **2** in THF showed similar broad absorption with the lowest energy peak at 313 and 310 nm (Figure 4a; Figure S3, Supporting Information), respectively, originating from π–π^* electron transition of the terpyridine units,[11] and the optical bandgap for the two ligands was also comparable (**1**, 3.30 eV; **2**, 3.24 eV). We attributed the broad absorption to sub-energy bands due to weak intra-ligand charge transfer in the carbazole-terpyridine acceptor–donor–acceptor triads with a phenylene bridge, a similar but larger splitting (ca. 80 nm) has been reported for terpyridine units in a Zn-linked pentamer of 3,6-di([2,2′:6′,2″-terpyridin]-4′-yl)-9-hexyl-9H-carbazole.[11] In the fluorescence spectra, the emission peak of **1** appeared at longer wavelength (401 nm) than that of **2** (386 nm; Figure S3, Supporting Information) possibly due to aggregation through H-bonding. Furthermore, the emission profile of both **1** and **2** showed a long tail at longer wavelengths (ca. 450 nm). Upon changing the solvent to ACN, the emission of **1** showed an excitation wavelength-dependent profile (Figure 4b), in which the relative intensity of longer wavelength shoulder peak at 459 nm to peak at 401 increased as the excitation wavelength increased from 310 to 360 nm. No such phenomenon was observed for **1** in THF, while **2** was insoluble in acetonitrile. This can be explained by the different polarity of the solvents, in

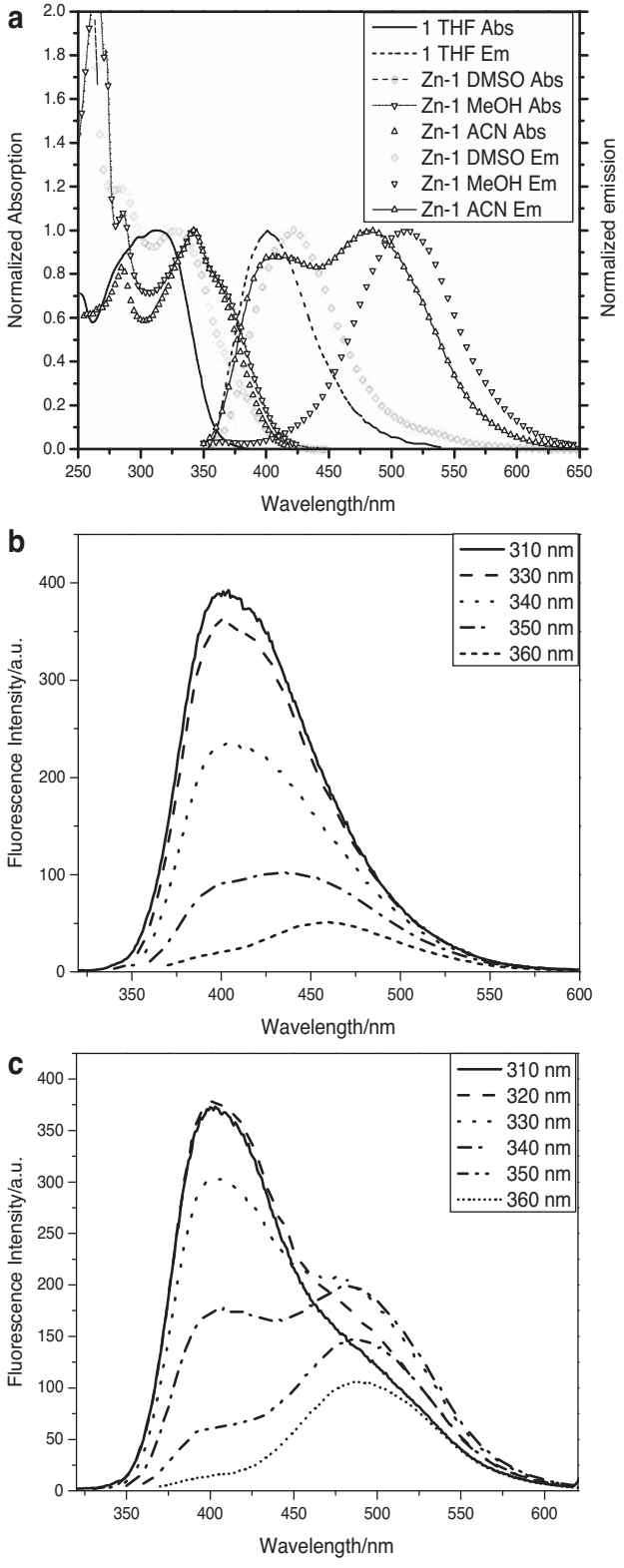

Figure 4. a) Normalized absorption and fluorescence spectra of **1** in THF and **Zn-1** in DMSO, MeOH, ACN; b) excitation wavelength-dependent emission of **1** in ACN; c) excitation wavelength-dependent emission of **Zn-1** in ACN. Concentration for absorption: 10^{-5} M; concentration for emission: 10^{-7} M.

that the more polar acetonitrile can stabilize the intermediate intra-ligand charge transfer state and thus facilitate the emission from 459 nm, as has been reported in a recent study of dual solvent-dependent emission properties of carbazole–terpyridine donor–acceptor luminophores with terpyridine units linked to the N-position of carbazole,[25] and in a study by us on metallo-copolymers containing unit **1**.[26]

Of the metallocycles, **Zn-1** showed solvent-dependent absorption and emission in dimethyl sulfoxide (DMSO), ACN, and MeOH (Figure 4a). A sharp absorption due to the carbazole unit at 285 nm was observed in all three solvents, while the terpyridine unit exhibited a single peak at 329 nm in DMSO, and a red-shifted main peak at 342 nm with a shoulder peak at 362 nm in ACN and MeOH, which were all in the same region with the absorption area of free ligand **1** due to full d-electrons of Zn ions and lack of metal–ligand charge transfer. When excited at 340 nm in very dilute concentration (ca. 10^{-7} M), the emission in DMSO and MeOH, respectively, appeared as a single peak centered at 412 nm (blue fluorescence) or 512 nm (green fluorescence), while double emission at 403 and 483 nm was observed in ACN. Moreover, the relative intensity of the two emission peaks was dependent on the excitation wavelength (Figure 4c). As the excitation wavelength increased from 310 to 360 nm, the emission intensity at 403 nm decreased and that at 483 nm increased. Moreover, the excitation spectra with emission wavelength at 403 and 483 nm showed different peaks at 320 and 340 nm (Figure S4, Supporting Information), confirming the existence of two different excitation energy bands. Compared with **1**, the emission from an intra-ligand charge transfer state of **Zn-1** was more notable, due to coordination resulted locking of the terpyridine in a cisoid orientation.

2.3. Fluorescence Titration of Zn-1 with C_{60}

Fluorescence titration of **Zn-1** was carried out by monitoring fluorescence intensity at 403 nm (excitation at 330 nm) in dilute ACN upon stepwise addition of C_{60} (ACN:chlorobenzene 1:1). Rapid quenching was observed (Figure 5a), and the high Stern–Volmer binding constant calculated from linear fit was 3.2×10^5 M^{-1} (Figure 5b). Monotonic increase in the stoichiometry plot inferred no formation of a stable host–guest inclusion,[12] and effective charge transfer between **Zn-1** and C_{60} molecules was suggested as a reason for the fast fluorescence quenching.[27]

2.4. Electrochemical Properties

The electrochemical properties were characterized by cyclic voltammetry (CV) using 0.1×10^{-3} M solutions of **1** (THF) and **Zn-1** (ACN) with 0.1 M tetra(*n*-butyl)ammonium hexafluorophosphate (Bu_4NPF_6) as electrolytes at 25 °C versus

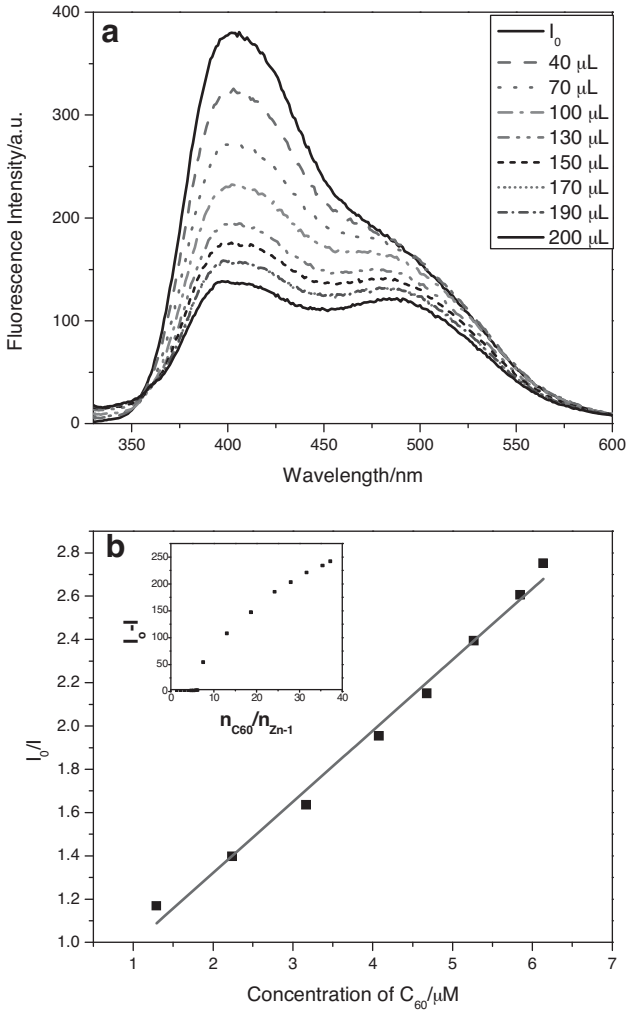

Figure 5. a) Fluorescence titration of 3 mL **Zn-1** (1.76×10^{-7} M, ACN) with stepwise addition of C_{60} (9.8×10^{-5} M, acetonitrile:chlorobenzene 1:1). b) Stern–Volmer plot, inset: stoichiometry plot.

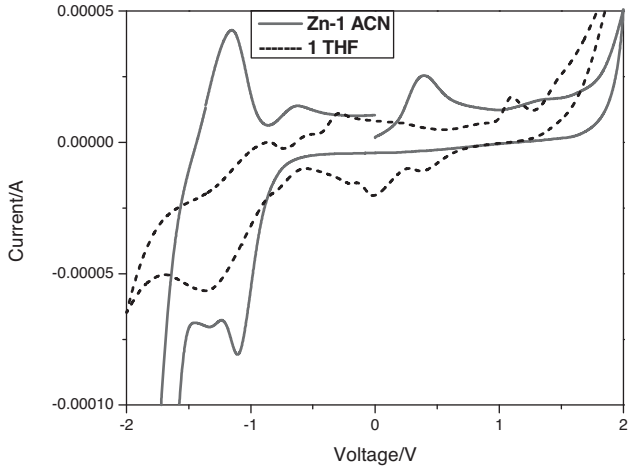

Figure 6. CV curves of **1** in THF and **Zn-1** in ACN. Working electrode: carbon electrode, counter electrode: platinum wire, reference electrode: saturated Ag/AgCl, electrolytes: 0.1 M Bu_4NPF_6, scan rate: 0.1 mV s^{-1}.

Ag/AgCl, and all the oxidation and reduction half-reactions were found irreversible (Figure 6). For **1**, the anodic peak at 1.09 V (peak value) originated from carbazole unit, and the irreversibility was caused by the formation of coupling radical cations according to literature precedents.[25] The other three pairs of signals were assigned to the sequential terpyridine-associated events with the strongest cathodic signal at –1.36 V, which was more positive than reported values and can be reasonably explained by the outcome of electronic interaction between electron-rich carbazole and electron-withdrawing terpyridine moieties.[8] For a three-step scan for **Zn-1** (0 to 2 V, 2 to –2 V, and –2 to 0 V), the oxidation events showed a signal at 0.387 V and another relatively weak peak at 1.35 V for carbazole unit, and the predominating cathodic reduction signal was recorded at –1.11 V for terpyridine when scanning toward negative potential. Moreover, the appearance of the second reduction peak (–1.31 V) during negative scanning and the following peaks (–1.15 V, –0.63 V) during forward sweep was dependent on the scan range, with only the main peak (–1.11 V) observed when changing the scan range to two-step sweeping (0 to –1.6 V and then to 0 V; Figure S5, Supporting Information). Such differences probably arose from the insoluble neutral substance adhered on the surface of electrode, which was formed after two one-electron oxidation events and two one-electron reduction events with the additional second reduction during the three-step scanning.[8] The HOMO/LUMO energy levels of **Zn-1** as determined by CV are –4.78 eV ($-(E_{ox} + 4.4)$ eV) and –3.29 eV ($-(E_{red} + 4.4)$ eV), respectively, which were calculated[28] from the onset potentials of the first oxidation (0.387 V) and the first reduction (–1.11 V). The higher LUMO energy of **Zn-1** as compared with that of C_{60} (–4.5 eV)[29] suggest charge transfer between **Zn-1** and C_{60} is favorable, which is consistent with the aforementioned rapid fluorescence quenching.

The diffusion coefficient of **Zn-1** was estimated using the Randles–Sevcik equation with data collected by cathodic scans at various scan rates (30–100 mV s^{-1}) (Figure S5, Supporting Information), to be 7.16×10^{-8} cm^2 s^{-1}, which was in the same order of magnitude as literature-reported values for similar structures.[11]

2.5. Thermal Properties

The thermal properties were examined by thermogravimetric analysis (TGA) and differential scanning calorimetry (DSC). Under nitrogen atmosphere, **1** started to decompose at 260 °C (5% weight loss) and totally decomposed at 600 °C, while **Zn-1** started to decompose at 300 °C and maintained 30% weight at 600 °C, which was comparable to the weight ratio of metal salt ($Zn(PF_6)_2$) (Figure 7a). The

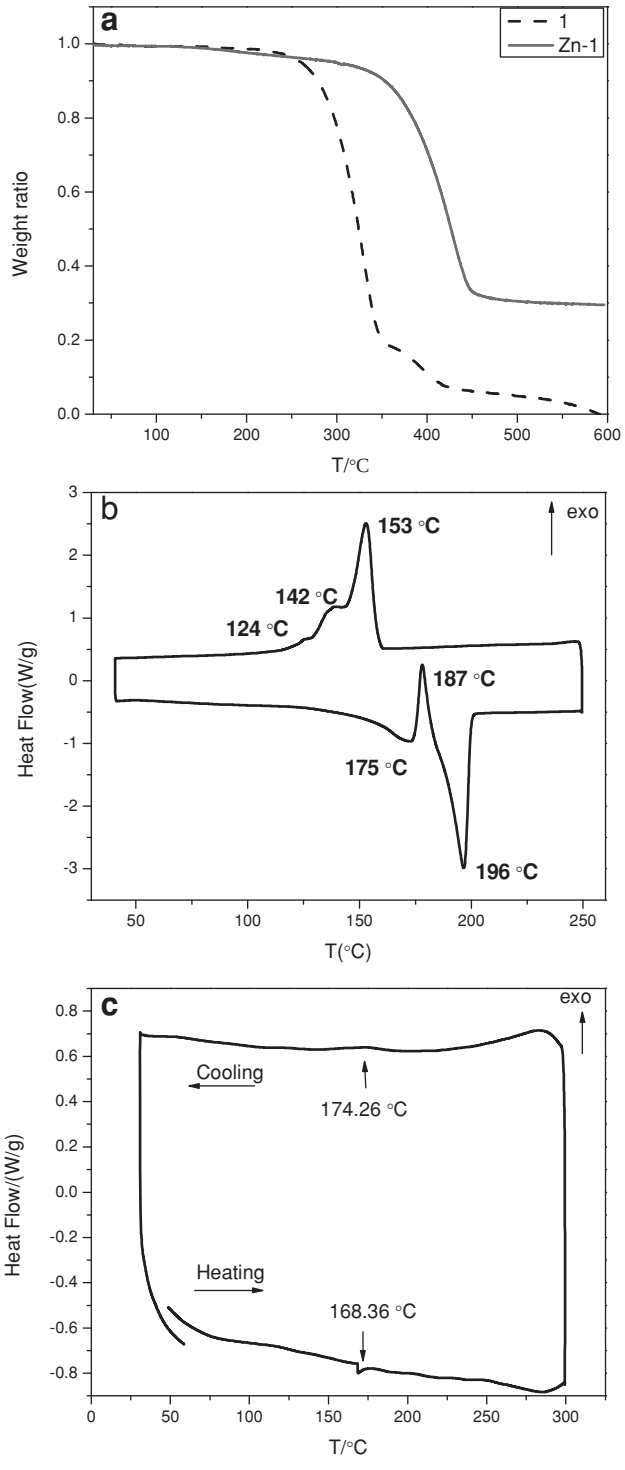

Figure 7. a) TGA spectra of **1** and **Zn-1**; b) and c) DSC spectra of **1** and **Zn-1**, respectively. The experiments were carried out in N_2 atmosphere, and the temperature was increased and decreased at 10 °C min^{-1}.

better heat stability of **Zn-1** was attributed to the presence of metal ions and the structural rigidity of the metallocycle. In DSC, **1** exhibited two endothermal (175.0, 196.6 °C) and one exothermal signal (187.3 °C) during heating cycle and three exothermal signals (153.0, 135.4, 124.4 °C) during cooling (Figure 7b), while only a shallow endothermal peak (168.3 °C) and a negligible exothermal signal appeared during heating for **Zn-1** (Figure 7c). By comparing the molecular structures of **1** and **Zn-1**, the weak broad endothermal signal at 175.0 °C (heating) in **1** was assigned to the breaking down of intermolecular H-bonds between NH functional groups, which occurred in a similar temperature region for the more rigid **Zn-1**. The notable endothermal peak at 187.3 °C for **1** was probably from the formation of H-bonds between NH groups and pyridine N atoms. The pair of sharp signals at 196 °C (heating) and 153 °C (cooling) for **1** were believed to arise from configuration changes from the all-*trans*-configuration of pyridine N-atoms in metal-free ligand, which was absent in **Zn-1** because of the fixed all-*cis*-configuration produced by coordination.

Moreover, no melt phenomena were observed in thin films drop cast from THF solutions of **1** after heating up to 220 °C under optical microscope, while nematic liquid crystal phases appeared upon slow cooling (10 °C min^{-1}) the film to room temperature under a cross-polarized microscope (POM, Figure S6, Supporting Information). In contrast, pristine **Zn-1** powder showed smectic phases without heat treatment (Figure 8a), which implied an ordered arrangement of the molecules in the solid state.

2.6. Molecular Packing

The crystallinity of **Zn-1** was further characterized using powder XRD (Figure S7, Supporting Information), which showed a series of peaks with d-spacing displayed in multifold relationships (Table S1, Supporting Information). Such self-organization order was remarkable in view of the nonplanarity of the metallocycles.[21] Moreover, an atomic force microscopy (AFM) study of **Zn-1** prepared by slow solvent evaporation (MeOH, 10^{-7} M) on silica substrate showed a micrometer-scale 2D nanofilm ($h = 2.2$ nm) (Figure 8b), while a TEM study of **Zn-1** powder prepared by dispersion in MeOH showed overlapped layers (Figure 8c). Upon changing the solvent to a mixture of ACN:MeOH (1:9, ca. 10^{-7} M) so as to manipulate the solvent evaporation rate, curly thin layers of **Zn-1** with an interlayer distance ca. 5 nm were observed under transmission electron microscopy (TEM) (Figure 8d). The layering assembly behaviors implied both in-plane and out-of-plane H-bonds existed among the macrocycles, which feature good hole transporting property for the carbazole units.

3. Conclusion

Zinc ion-mediated assembly of angular carbazole-based bisterpyridine ligands variously produced a well-defined

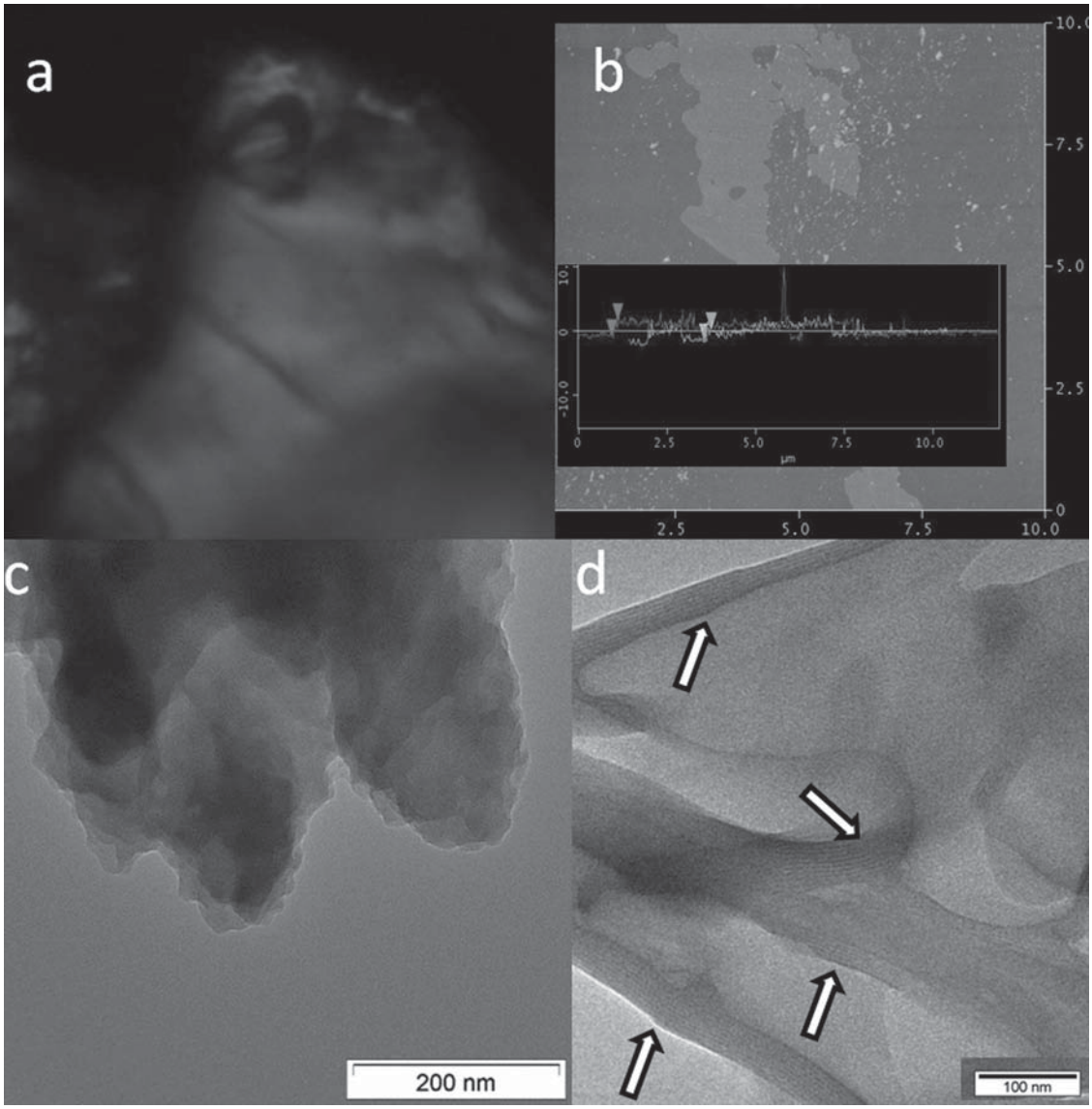

Figure 8. a) POM image of **Zn-1** powder (50 μm × 50 μm) under dark field; b) AFM image of **Zn-1** prepared by slow evaporation of dilute MeOH solution (10^{-7} M) on silica substrate (10 μm × 10 μm); c) TEM image of Zn-1 powder; d) TEM image of **Zn-1** prepared from dilute solution of mixed solvent (ACN:MeOH 1:9, 10^{-7} M).

pentameric structure **Zn-1** for a ligand with an NH group capable of intermolecular H-bond interactions, and a two-component mixture **Zn-2** for a ligand with a dodecyl chain, which prevents such interactions. Fluorescence properties of **Zn-1** revealed solvent-dependent profile with blue emission from DMSO and green emission from MeOH, and distinct tunable dual emission in ACN with relative enhancement in the green emission to the blue emission upon increasing excitation wavelength (320–360 nm). The two emission bands originated from a localized excitation state and an intra-ligand charge transfer band. Electrochemical experiments showed respective oxidation and reduction half-reactions for carbazole and terpyridine moieties. Fluorescence quenching of **Zn-1** with C_{60} showed a very high binding constant. The existence of zinc ions and intermolecular H-bond in molecule **Zn-1** resulted in better heat tolerance and fewer phase transitions compared with metal-free ligand **1**. Molecular packing of **Zn-1** showed promising nanoscale 2D-layered order in powder XRD, AFM, and TEM. Further theoretical molecular orbital study, molecular modeling, and OFET studies are planned to fully understand and evaluate the properties of the pentameric complex **Zn-1**.

4. Experimental Section

The terpyridine boronate[30,31] and 3,6-dibromo-9-decylcarbazole[16,32] were made by literature methods. All other starting

materials, reagents, and solvents used in this project were purchased from commercial sources (e.g., Sigma–Aldrich, Alfa Aesar, and so on), and used as obtained. All the reactions were carried out under an inert N_2 atmosphere. Mass spectra were recorded using Shimadzu Axima matrix-assisted laser desorption/ionization time-of-flight mass spectrometer (MALDI-TOF-MS) without matrix, or ThermoFinigan LCQ Fleet Mass Spectrameter with quadrupole ion trap. Absorption spectra were taken on a UV–vis recording spectrophotometer (Shimadzu UV-2501PC). Fluorescent measurements were taken on a spectrofluorophotometer (Shimadzu RF-5301PC). CV was performed on a CHI660D electrochemical analyzer with a three-electrode cell. TGA experiments were performed on TA TGA-Q500 with a dynamic heat rate (10 °C min^{-1}) under N_2 atmosphere (50 mL min^{-1}). DSC measurements were performed on TA DSC-Q10 with dynamic heating and cooling rate (10 °C min^{-1}) under N_2 atmosphere (50 mL min^{-1}). Polarized microscope images were recorded on an Olympus machine. XRD scanning (5° to 50°) was studied by Bruker AXS D8 Advance X-ray diffractometer. AFM images were recorded by AFM DI 3000 machine. TEM images were recorded on a Carl Zeiss Libra 120 machine.

1: A stirred mixture of 3,6-dibromo-9H-carbazole (0.50 g, 1.5 mmol), the terpyridyl boronate (1.30 g, 3.0 mmol), aqueous K_2CO_3 (2 M, 5 mL), and $Pd(PPh_3)_4$ (98.9 mg, 0.08 mmol) dissolved in toluene (20 mL) was refluxed for 3 d. The solvent was removed under reduced pressure and the residue was extracted with DCM/H_2O. The combined extract was dried over Na_2SO_4, filtered, concentrated, and then purified through column chromatography (neutral Al_2O_3, eluting solvent: ^{n}hexane:DCM:MeOH 100:50:1) to afford 1 as off-white solid (yield: 350 mg, 45%). ^{1}H NMR (400 MHz, $CDCl_3$, δ) 8.76 (s, 4H, Tpy$H^{3',5'}$), 8.75 (d, 4H, J = 4 Hz, Tpy$H^{6',6''}$), 8.69 (d, 4H, J = 8 Hz, Tpy$H^{3',3''}$), 7.95 (d, 4H, J = 8 Hz, Ph-H), 7.91 (t, 4H, J = 8 Hz, Tpy$H^{4',4''}$), 7.76 (d, 4H, J = 8 Hz, Ph-H), 7.42 (d, 2H, J = 4 Hz, Car-4H), 7.38–7.33 (m, 6H, Tpy$H^{5',5''}$, Car-1H), 7.13 (t, 2H, J = 4 Hz, Car-2H);^{13}C NMR (100 MHz, $CDCl_3$, δ) 156.24, 155.99, 149.57, 149.14, 136.92, 135.11, 128.19, 127.83, 126.31, 125.34, 123.88, 121.42, 118.56; MS (MALDI-TOF) m/z: calcd for $C_{54}H_{35}N_7$, 781.90; found, 780.40 ([M–H]$^-$).

$[Zn_5(1)_5][10PF_6^-]$ (Zn-1): $Zn(OAc)_2{\cdot}2H_2O$ (81.9 mg, 0.37 mmol) was added to a stirred solution of **1** (298.4 mg. 0.38 mmol) in NMP (14 mL), then the mixture was heated to 100 °C for 48 h. A slight excess of NH_4PF_6 was added, and stirred for another 0.5 h before cooling down. The cooled solution was then added dropwise to large amount of MeOH, and stored at –20 °C. The precipitation was collected through filtration and further washed in refluxing DCM and MeOH to afford Zn-1 as an off-white solid (yield: 124 mg, 29%). ^{1}H NMR (400 MHz, d_3-ACN, δ) 9.00 (s, 4H, Tpy$H^{3',5'}$), 8.74 (d, 4H, J = 8 Hz, Tpy$H^{3',3''}$), 8.26 (d, 4H, J = 8 Hz, Ph-H), 8.20 (t, 4H, J = 8 Hz, Tpy$H^{4',4''}$), 8.06 (d, 4H, J = 8 Hz, Ph-H), 7.85 (d, 4H, J = 4 Hz, Tpy$H^{6',6''}$), 7.68 (d, 2H, J = 4 Hz, Car-4H), 7.52 (d, 2H, J = 4 Hz, Car-1H), 7.42 (t, 4H, J = 8 Hz, Tpy$H^{5',5''}$), 7.25 (t, 2H, J = 4 Hz, Car-2H);^{13}C NMR (100 MHz, d3-ACN, δ) 150.62, 148.80, 148.71, 142.14, 137.74, 129.61, 128.37, 127.66, 127.42, 125.83, 124.01, 122.00; ESI-MS (Figure S1, Supporting Information) m/z: 1662.91 $[M–H^+\text{-}4PF_6^-\text{-}6HF]^{3+}$ (Calcd. m/z = 1661.72), 1324.54 $[M\text{-}2PF_6^-\text{-}2F^-\text{-}3HF]^{4+}$ (Calcd. m/z = 1324.52), 992.57 $[M\text{-}5PF_6^-]^{5+}$ (Calcd. m/z = 992.24), 958.70 $[M\text{-}5PF_6^-\text{-}2HF]^{5+}$ (Calcd. m/z = 959.04), 886.34 $[M\text{-}2PF_6^-\text{-}4F^-]^{6+}$ (Calcd. m/z = 886.68), 894.65 $[M\text{-}PF_6^-\text{-}5F^-\text{-}4HF]^{6+}$ (Calcd. m/z = 894.34), 674.66 $[M\text{-}6PF_6^-\text{-}2F^-\text{-}H^+\text{-}3HF]^{7+}$ (Calcd. m/z = 673.89), 590.87 $[M\text{-}6PF_6^-\text{-}2F^-\text{-}3HF]^{8+}$ (Calcd. m/z = 589.78), 499.95 $[M\text{-}8PF_6^-\text{-}F^-]^{9+}$ (Calcd. m/z = 500.80), 423.58 $[M\text{-}10PF_6^-]^{10+}$ (Calcd. m/z = 423.64).

2: A stirred mixture of 3,6-dibromo-9-decyl-9H-carbazole (305.1 mg, 0.6 mmol), the terpyridyl boronate (784.6 mg, 1.8 mmol), aqueous K_2CO_3 (2 M, 3 mL), and $Pd(PPh_3)_4$ (75.4 mg, 0.06 mmol) dissolved in THF (8 mL) was refluxed for 5 d. The solvent was removed under reduced pressure and the residue was extracted with DCM/H_2O. The combined extract was dried ($MgSO_4$), filtered, concentrated, and then purified through column chromatography (neutral Al_2O_3, eluting solvent: ^{n}hexane:DCM:triethylamine 100:50:1) to afford **2** as an off-white solid (yield: 160 mg, 28%). ^{1}H NMR (400 MHz, $CDCl_3$, δ) 8.85 (s, 4H, Tpy$H^{3',5'}$), 8.78 (d, 4H, J = 4 Hz, Tpy$H^{6',6''}$), 8.72 (d, 4H, J = 8 Hz, Tpy$H^{3',3''}$), 8.49 (s, car-4H), 8.08 (d, 4H, J = 8 Hz, Ph-H), 7.93 (m, 8H, Tpy$H^{4',4''}$, Ph-H), 7.84 (d, 2H, J = 8 Hz, Car-1H), 7.53 (d, 2H, J = 8 Hz, Car-2H), 7.40 (t, 4H, J = 8 Hz, Tpy$H^{5',5''}$), 4.39 (t, 2H, J = 8 Hz, NCH_2), 1.95 (t, 2H, J = 8 Hz, CH_2), 1.42 (m, 18H, CH_2), 0.88 (t, 3H, J = 4 Hz, CH_3);^{13}C NMR (100 MHz, $CDCl_3$, δ) 150.12, 148.82, 142.84, 140.68, 137.37, 136.15, 131.60, 127.80, 125.39, 123.96, 123.59, 121.65, 119.05, 109.27, 31.93, 29.72, 29.63, 27.37, 22.71, 14.15; MS (MALDI-TOF) m/z: calcd for $C_{66}H_{59}N_7$, 950.22; found, 951.16 ([M+H]$^+$).

Zn-2: $Zn(OAc)_2{\cdot}2H_2O$ (10.9 mg, 0.05 mmol) was added to a stirred solution of **2** (45.2 mg. 0.05 mmol) in NMP (5 mL), then the mixture was heated to 100 °C for 48 h. A slight excess of NH_4PF_6 was added, and stirred for another 0.5 h before cooling down. The cooled solution was then added dropwise to large amount of MeOH, and stored at –20 °C. Precipitation was collected through filtration and further washed in refluxing DCM and MeOH to afford **Zn-2** as a brown solid (yield: 15 mg, 23%). ^{1}H NMR (400 MHz, d3-ACN, δ) 9.11 (s, 3H, Tpy$H^{3',5'}$), 9.09 (s, 1H, Tpy$H^{3',5'}$), 8.78 (m, 6H, Tpy$H^{3',3''}$, car-4H), 8.41 (t, 4H, J = 6 Hz, Tpy$H^{4',4''}$), 8.26 (m, 8H, Ph-H), 8.08 (d, 2H, J = 8 Hz, car-1H), 7.93 (d, 3H, J = 4 Hz, Tpy$H^{6',6''}$), 7.86 (d, 1H, J = 4 Hz, Tpy$H^{6',6''}$), 7.79 (d, 2H, J = 8 Hz, Car-2H), 7.44 (t, 4H, J = 6 Hz, Tpy$H^{5',5''}$), 4.55 (t, 2H, J = 6 Hz, NCH_2), 1.42–1.26 (br, 18H, CH_2), 0.91 (t, J = 6 Hz, 3H, CH_3).

Supporting Information

Supporting Information is available from the Wiley Online Library or from the author.

Acknowledgements: Y.G. thanks NTU for the granting of a postgraduate Research Scholarship. The authors acknowledge the National Research Foundation for funding through CRP Grant 5–2009–04 "Towards Efficient Sunlight Harvesting."

Received: November 25, 2013; Revised: February 11, 2014; Published online: March 25, 2014; DOI: 10.1002/macp.201300737

Keywords: dual emission; H-bond; long-range order; macrocycle; tunable emission

[1] R. Chakrabarty, P. S. Mukherjee, P. J. Stang, *Chem. Rev.* **2011**, *111*, 6810.
[2] A. Wild, A. Winter, F. Schlutter, U. S. Schubert, *Chem. Soc. Rev.* **2011**, *40*, 1459.
[3] Y.-T. Chan, X. Li, M. Soler, J.-L. Wang, C. Wesdemiotis, G. R. Newkome, *J. Am. Chem. Soc.* **2009**, *131*, 16395.

[4] S. Perera, X. Li, M. Guo, C. Wesdemiotis, C. N. Moorefield, G. R. Newkome, *Chem. Commun.* **2011**, *47*, 4658.
[5] X. Lu, X. Li, J.-L. Wang, C. N. Moorefield, C. Wesdemiotis, G. R. Newkome, *Chem. Commun.* **2012**, *48*, 9873.
[6] J.-L. Wang, X. Li, X. Lu, I. F. Hsieh, Y. Cao, C. N. Moorefield, C. Wesdemiotis, S. Z. D. Cheng, G. R. Newkome, *J. Am. Chem. Soc.* **2011**, *133*, 11450.
[7] X. Lu, X. Li, Y. Cao, A. Schultz, J.-L. Wang, C. N. Moorefield, C. Wesdemiotis, S. Z. D. Cheng, G. R. Newkome, *Angew. Chem Int. Ed.* **2013**, *52*, 7728.
[8] G. R. Newkome, T. J. Cho, C. N. Moorefield, R. Cush, P. S. Russo, L. A. Godínez, M. J. Saunders, P. Mohapatra, *Chem. Eur. J.* **2002**, *8*, 2946.
[9] G. R. Newkome, P. Wang, C. N. Moorefield, T. J. Cho, P. P. Mohapatra, S. Li, S.-H. Hwang, O. Lukoyanova, L. Echegoyen, J. A. Palagallo, V. Iancu, S.-W. Hla, *Science* **2006**, *312*, 1782.
[10] Y.-T. Chan, X. Li, J. Yu, G. A. Carri, C. N. Moorefield, G. R. Newkome, C. Wesdemiotis, *J. Am. Chem. Soc.* **2011**, *133*, 11967.
[11] S.-H. Hwang, P. Wang, C. N. Moorefield, L. A. Godinez, J. Manriquez, E. Bustos, G. R. Newkome, *Chem. Commun.* **2005**, *0*, 4672.
[12] D. C. Flynn, G. Ramakrishna, H.-B. Yang, B. H. Northrop, P. J. Stang, T. Goodson, *J. Am. Chem. Soc.* **2010**, *132*, 1348.
[13] C. Y. Lee, O. K. Farha, B. J. Hong, A. A. Sarjeant, S. T. Nguyen, J. T. Hupp, *J. Am. Chem. Soc.* **2011**, *133*, 15858.
[14] H.-J. Son, S. Jin, S. Patwardhan, S. J. Wezenberg, N. C. Jeong, M. So, C. E. Wilmer, A. A. Sarjeant, G. C. Schatz, R. Q. Snurr, O. K. Farha, G. P. Wiederrecht, J. T. Hupp, *J. Am. Chem. Soc.* **2012**, *135*, 862.
[15] K. Brunner, A. van Dijken, H. Borner, J. Bastiaansen, N. M. M. Kiggen, B. M. W. Langeveld, *J. Am. Chem. Soc.* **2004**, *126*, 6035.
[16] J. Kim, Y. S. Kwon, W. S. Shin, S.-J. Moon, T. Park, *Macromolecules* **2011**, *44*, 1909.
[17] B. Souharce, C. J. Kudla, M. Forster, J. Steiger, R. Anselmann, H. Thiem, U. Scherf, *Macromol. Rapid Commun.* **2009**, *30*, 1258.
[18] Z.-S. Wang, N. Koumura, Y. Cui, M. Takahashi, H. Sekiguchi, A. Mori, T. Kubo, A. Furube, K. Hara, *Chem. Mater.* **2008**, *20*, 3993.
[19] J. Li, A. C. Grimsdale, *Chem. Soc. Rev.* **2010**, *39*, 2399.
[20] J.-Y. Li, C.-Y. Chen, J.-G. Chen, C.-J. Tan, K.-M. Lee, S.-J. Wu, Y.-L. Tung, H.-H. Tsai, K.-C. Ho, C.-G. Wu, *J. Mater. Chem.* **2010**, *20*, 7158.
[21] S.-H. Jung, W. Pisula, A. Rouhanipour, H. J. Räder, J. Jacob, K. Müllen, *Angew. Chem Int. Ed.* **2006**, *45*, 4685.
[22] T. Vehoff, B. Baumeier, D. Andrienko, *J. Chem. Phys.* **2010**, *133*, 134901.
[23] J. R. Li, D. J. Timmons, H. C. Zhou, *J. Am. Chem. Soc.* **2009**, *131*, 6368.
[24] P. Wang, G. R. Newkome, C. Wesdemiotis, *Int. J. Mass Spectrom.* **2006**, *255*, 86.
[25] A. Baschieri, L. Sambri, I. Gualandi, D. Tonelli, F. Monti, A. D. Esposti, N. Armaroli, *RSC Adv.* **2013**, *3*, 6507.
[26] Y. G. T. He, R. Chen, L. Ma, D. Rajwar, Y. Wang, A. C. Grimsdale, H. Sun, *Macromolecules* **2014**, *47*, 1316.
[27] H. Xu, Y. Yang, Y.-Z. Zhu, J.-Y. Zheng, *Chin. J. Chem.* **2006**, *24*, 1589.
[28] J. Lohrman, C. Zhang, W. Zhang, S. Ren, *Chem. Commun.* **2012**, *48*, 8377.
[29] S. Duhm, H. Glowatzki, V. Cimpeanu, J. Klankermayer, J. P. Rabe, R. L. Johnson, N. Koch, *J. Phys. Chem. B* **2006**, *110*, 21069.
[30] W. Goodall, K. Wild, K. J. Arm, J. A. G. Williams, *J. Chem. Soc., Perkin Trans. 2* **2002**, 1669.
[31] E. Sariola-Leikas, M. Niemi, H. Lemmetyinen, A. Efimov, *Org. Biomol. Chem.* **2013**, *11*, 6397.
[32] S. Telitel, F. Dumur, T. Faury, B. Graff, M.-A. Tehfe, D. Gigmes, J.-P. Fouassier, J. Lalevée, *Beilstein J. Org. Chem.* **2013**, *9*, 877.